International Journal of Innovative
Computing, Information and Control
Volume **10**, Number **6**, December **2014**

ICIC International ©2014 ISSN 1349-4198
pp. 2011–2023

DECOUPLED TERMINAL SLIDING-MODE CONTROL FOR A CLASS OF UNDER-ACTUATED MECHANICAL SYSTEMS WITH HYBRID SLIDING SURFACES

Guoliang Zhao, Can Zhao and Junting Cheng

Modern Manufacture Engineering Center
Heilongjiang University of Science and Technology
No. 2468, Puyuan Road, Songbei District, Harbin 150027, P. R. China
ocnzhao@gmail.com

Received December 2013; revised April 2014

Abstract. *This paper presents two fast decoupled sliding-mode controllers with hybrid sliding surfaces for a class of under-actuated mechanical systems. The proposed method not only exhibits a simpler structure compared with the existing decoupled control methods, but also eliminates the need for using fuzzy rules without degradation in performance. A cart-pole system and translational oscillations by a rotational actuator (TORA) system are simulated, and experiments on cart-pole system are carried out. Simulation results and experimental results have shown a considerable improvement of the proposed method in terms of a faster dynamic response as compared with the existing decoupled sliding mode control methods.*

Keywords: Sliding-mode control, Decoupled sliding-mode control, Fast terminal sliding-mode control, Hybrid sliding surface

1. **Introduction.** Under-actuated mechanical systems such as cart-pole system, pendubot and TORA are systems with fewer inputs than degrees of freedom. Under-actuated mechanical system control is a challenging task in engineering practice, and many existing control methods can be applied, such as sliding mode control [1-9], passivity based control [10], fuzzy control [11, 12] and optimal control [13, 14]. Recently, a decoupled sliding-mode control (DSMC) has been proposed for a class of under-actuated systems, and provides a simple way to decouple a class of fourth-order systems into two second-order subsystems. The auxiliary subsystem can be successfully incorporated into the main one via a two-level decoupling strategy [2]. For controlling three-stage cart-pole system and one-stage cart-pole system, an experience-based decoupling method with some mediate variables is applied [1]. To avoid singularity, Bayramoglu and Komurcugil propose a nonsingular decoupled terminal sliding mode control (NDTSMC) method [15], the convergence of the two subsystems to their equilibrium points in finite time can be guaranteed, and this is the same as TSMC [16]. However, the justification of the auxiliary sliding surface convergence has not been further studied. In the field of chaos control problem, a decoupled adaptive neuro-fuzzy sliding mode controller is studied [4]. For the TORA system, a decoupled self-tuning fuzzy sliding-mode controller design approach is proposed. Simulation results show that the states response converges faster than the previous reports [5]. Furthermore, an alternative decoupling approach termed as single-input decoupled fuzzy-logic control (SIDFLC) is also proposed as an improved version of the DSMC method [17].

In this paper, based on three given hybrid terminal sliding surfaces, a new fast decoupled terminal sliding-mode control (FDTSMC) scheme is presented, and singularity problem is eliminated by the carefully designed control law. Motivation of this work comes from the

fact that many other past-proposed controllers usually use the same sliding surface in the decoupled system design. Moreover, fuzzy rules are often employed in the time-varying sliding surfaces design to obtain faster convergence, and it is not an easy task to get a fine-tuning rule base [5]. In this paper, we remove the rule base and use the new hybrid sliding surface to get a faster convergence. Furthermore, convergence speed of the main sliding surface depends heavily on the auxiliary decoupled sliding surface's convergence speed; thus a fast reaching time sliding surface should be adopted to facilitate the overall convergence speed. The proposed FDTSMC has following advantages. (1) It controls a class of under-actuated systems well. (2) The convergence rate of the controlled system is faster than NDTSMC by using hybrid sliding surfaces. (3) Fuzzy rules are no longer needed in the FDTSMC design scheme; for the cart-pole system and TORA system, better results can be obtained. (4) The simulations and experimental results are done under the restriction that control input is bounded by 40 (N) for cart-pole system, and settling time for states of TORA should be less than 30 (s) while the control input and the settling time are not explicitly presented in the existing literature. The newly proposed fast decoupled terminal sliding-mode controller may have potential application in many under-actuated systems, for example, micro aerial vehicles such as quadrotor helicopter [24], vertical takeoff and landing aircraft [23] and automated laboratory equipments' controller design.

The organization of this paper is given as follows. In Section 2, the systems and some preliminaries are presented. In Section 3, a fast decoupled terminal sliding mode control (FDTSMC) scheme for a class of under-actuated mechanical system is presented. Then, based on three different terminal sliding surfaces, two fast decoupled sliding mode control methods are proposed and some properties are studied. In Section 4, the proposed methods are used to control a cart-pole system and TORA system; simulation results are presented and compared with the NDTSMC. Experimental results are also employed to verify the effectiveness of the two fast decoupled terminal sliding-mode controllers. Finally, the conclusion is provided in Section 5.

2. **Problem Statement and Preliminaries.** Consider the following system

$$\dot{x}_1 = x_2, \tag{1}$$
$$\dot{x}_2 = f_1(\mathbf{x}, t) + b_1(\mathbf{x}, t)u(t) + d_1(t), \tag{2}$$
$$\dot{x}_3 = x_4, \tag{3}$$
$$\dot{x}_4 = f_2(\mathbf{x}, t) + b_2(\mathbf{x}, t)u(t) + d_2(t), \tag{4}$$

where $\mathbf{x} = [x_1, x_2, x_3, x_4]^T$ is the state vector, $f_1(\mathbf{x}, t), b_1(\mathbf{x}, t), f_2(\mathbf{x}, t)$ and $b_2(\mathbf{x}, t)$ are nonlinear functions representing system dynamics, $u(t)$ is the control input, $d_1(t)$ and $d_2(t)$ represent external disturbances, $|d_1(t)| < d, |d_2(t)| < d$ and $d \geq 0$. Models of this type can describe a great variety of systems. Most of them are under-actuated systems, to name a few, under-actuated robot manipulators [21], translational oscillator with a rotational actuator (TORA) [22], cart-pole system [1], the vertical takeoff and landing (VTOL) aircraft [23], ball and beam system [25], and quadrotor helicopter [24].

System (1)-(4) can be partitioned as the following subsystem A

$$\dot{x}_1 = x_2, \tag{5}$$
$$\dot{x}_2 = f_1(\mathbf{x}, t) + b_1(\mathbf{x}, t)u(t) + d_1(t), \tag{6}$$

and subsystem B

$$\dot{x}_3 = x_4, \tag{7}$$
$$\dot{x}_4 = f_2(\mathbf{x}, t) + b_2(\mathbf{x}, t)u(t) + d_2(t). \tag{8}$$

The main target is to stabilize subsystem A (or B), it is also important to consider the information from subsystem B (or A) as secondary, and a mechanism is needed to reflect this information between subsystem A and subsystem B. Like the strategy proposed by Zhang et al. [1] and Lo and Kuo [2], an intermediate variable z is utilized to achieve this target. In this way, the subtarget of B (or A) is embedded to the main target through the intermediate variable z. Both primary and secondary targets can be achieved simultaneously.

3. **Fast Decoupled Terminal Sliding Mode Control.** To demonstrate the fast convergence performance of the above mentioned fast decoupled sliding surface, we consider the following three sliding surfaces:

$$s_1 = \dot{x} + \lambda_1 sig^{\gamma_1}(x - z) + \lambda_2 sig^{\gamma_2}(x - z) = 0, \tag{9}$$

$$s_2 = \dot{x} + x - z + \lambda_1 sig^{\gamma_1}(x - z) = 0, \tag{10}$$

$$s_3 = \dot{x} + \lambda_2 sig^{\gamma_2}(x - z) = 0, \tag{11}$$

where $\lambda_i\,(i = 1, 2)$ are positive coefficients, $\gamma_1 > 1$, $1 < \gamma_2 \leq 2$, $sig^{\gamma_i}(x_1 - z) = |x_1 - z|^{\gamma_i} sgn(x_1 - z)$, $sgn(\cdot)$ is the signum function, and z is an intermediate variable.

Example 3.1. *The fast decoupled terminal sliding surface functions designed by (9) are described in the following form:*

$$\sigma_1 = x_2 + \lambda_1 sig^{\gamma_1}(x_1 - z) + \lambda_2 sig^{\gamma_2}(x_1 - z), \tag{12}$$

$$\sigma_2 = x_3 + \lambda_3 sig^{\gamma_3}(x_4) + \lambda_4 sig^{\gamma_4}(x_4), \tag{13}$$

where z is an intermediate variable and will be defined later, λ_i $(i = 1, 2, 3, 4)$ are positive coefficients, $1 < \gamma_i = \frac{q_2}{p_2}\,(i = 1, 3)$, $1 < \gamma_i = \frac{q_1}{p_1} \leq 2\,(i = 2, 4)$, where p_1, p_2, q_1, q_2 are odd numbers, and z is a bounded oscillatory signal decaying to zero.

Remark 3.1. *Let $z = 0$, the newly proposed sliding surfaces are an extension of $s_1 = \dot{x} + \lambda_1 sig^{\gamma_1}(x) + \lambda_2 sig^{\gamma_2}(x)$ and $s_2 = \dot{x} + x + \lambda_1 sig^{\gamma_1}(x)$ which are named as FTSM by Yang and Yang* [19]*, and the sliding surface s_3 is adopted from Bayramoglu* [15]*. (9)-(11) are the modified version which can be obtained by incorporating an intermediate variable z into the sliding surface, respectively.*

Remark 3.2. *By solving the differential equation $\sigma_1 = 0$, $x_1 - z$ will be reached in finite time which is given by*

$$\begin{aligned} T_{s1} = \int_0^{|x_z(0)|} \frac{1}{\lambda_1 (x_1 - z)^{\gamma_1} + \lambda_2 (x_1 - z)^{\gamma_2}} dx_1 = \frac{|x_z(0)|^{1-\gamma_1}}{1 - \gamma_1} \lambda_1^{-1} \\ \cdot F\left(1, \frac{\gamma_1 - 1}{\gamma_1 - \gamma_2}; \frac{2\gamma_1 - \gamma_2 - 1}{\gamma_1 - \gamma_2}; -\lambda_2 \lambda_1^{-1} |x_z(0)|^{\gamma_2 - \gamma_1}\right), \end{aligned} \tag{14}$$

where $x_z(0)$ is the initial value of $x_1 - z$ at $t = t_r$ in the fast terminal sliding mode, $F(\cdot)$ denotes Gauss Hypergeometric function [20]*, and the conditions of λ_1, λ_2, γ_1, γ_2 induce that $F(\cdot)$ will guarantee convergence. The results can also be verified by computer algebra systems.*

Now, setting the derivative of (12) to zero, it results

$$\dot{\sigma}_1 = \dot{x}_2 + (\bar{\lambda}_1 |x_1 - z|^{\gamma_1 - 1} + \bar{\lambda}_2 |x_1 - z|^{\gamma_2 - 1})(x_2 - \dot{z}) = 0, \tag{15}$$

where $\bar{\lambda}_i = \lambda_i \gamma_i\,(i = 1, 2)$. Substituting $\dot{x}_2 = f_1(\mathbf{x}, t) + b_1(\mathbf{x}, t) u(t)$ into (15) and solving for $u(t)$, it yields

$$\hat{u}(t) = \frac{1}{b_1(\mathbf{x}, t)} \Big[- f_1(\mathbf{x}, t) - (\bar{\lambda}_1 |x_1 - z|^{\gamma_1 - 1} + \bar{\lambda}_2 |x_1 - z|^{\gamma_2 - 1})(x_2 - \dot{z}) \Big]. \tag{16}$$

Note that a switching control action is also needed to move the system states from an initial point to the sliding surface. Therefore, the control input in terms of equivalent control and switching control can be written as

$$u(t) = \hat{u}(t) - k_1\sigma_1 - k_2 sig^{\rho}(\sigma_1), \tag{17}$$

where $k_1 > 0, k_2 > 0$ and $0 < \rho < 1$.

Remark 3.3. *Note that $|x_1 - z|^{\gamma_2} \gg |x_1 - z|^{\gamma_1}$ when the state $x_1 - z$ is far away from zero. In this case, (12) can be approximated by $s_1 = x_2 + \lambda_2 sig^{\gamma_2}(x_1 - z)$. As $x_1 - z$ closes to zero, the dynamic is dominated by $s_1 = x_2 + \lambda_1 sig^{\gamma_1}(x_1 - z)$, from (15), we obtain*

$$\dot{x}_2 + \bar{\lambda}_1 |x_1 - z|^{\gamma_1 - 1} x_2 = \bar{\lambda}_1 |x_1 - z|^{\gamma_1 - 1} \dot{z}. \tag{18}$$

The solution of (18) is given by

$$x_2(t) = e^{-\bar{\lambda}_1 \int |x_1 - z|^{\gamma_1 - 1} dt} \left(x_2(0) + \bar{\lambda}_1 \int e^{\bar{\lambda}_1 \int |x_1 - z|^{\gamma_1 - 1} dt} |x_1 - z|^{\gamma_1 - 1} \dot{z} dt \right), \tag{19}$$

where $x_2(0)$ is the initial value of $x_2(t)$. Apparently, $x_2(t)$ decays to zero if and only if $x_1 = z$ and $\dot{z} = 0$.

Remark 3.4. *We can also define*

$$\sigma_1 = x_2 + x_1 + \lambda_2 sig^{\gamma_2}(x_1), \tag{20}$$

$$\sigma_2 = x_4 + (x_3 - z) + \lambda_3 sig^{\gamma_3}(x_3 - z) \tag{21}$$

as another sliding surfaces for subsystem A and subsystem B.

Fast decoupled terminal sliding mode control with hybrid sliding surfaces. In Figure 1, we notice that both s_1 and s_2 have faster convergence rate than s_3. The usual decoupled terminal sliding mode controller uses the same sliding surface in the subsystem A and subsystem B. For example, the sliding surface $s = \lambda_1 x_1 + x_2$ [5], and the nonsingular terminal sliding surface defined in (11) [15]. Motivated by this, we adopt two different sliding surfaces to implement the fast decoupled terminal sliding mode control scheme.

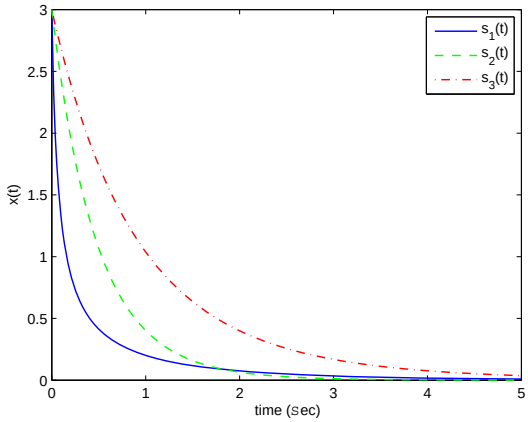

FIGURE 1. Comparison of s_1 ($\gamma_1 = 21/19, \gamma_2 = 7/3$), s_2 ($\gamma_1 = 21/19$), and s_3 ($\gamma_1 = 21/19$) when $z = 0$, $\lambda_1 = 1$ and $\lambda_2 = 3$

The fast decoupled terminal sliding surface functions with s_1 and s_2 (FDTSMC12) are described in the following form:

$$\begin{aligned} \sigma_1 &= x_2 + \lambda_1 sig^{\gamma_1}(x_1 - z) + \lambda_2 sig^{\gamma_2}(x_1 - z), \\ \sigma_2 &= x_4 + \lambda_3 sig^{\gamma_3}(x_3) + \lambda_4 x_3, \end{aligned} \tag{22}$$

where $\gamma_1 > 1$, $1 < \lambda_2 < 2$ and $\gamma_3 > 1$. Consider a Lyapunov function

$$V = \frac{1}{2}\sigma_1^2. \tag{23}$$

By Lyapunov theorem, we know that the system trajectories will be driven and attracted toward the sliding surface and remain sliding on it until origin is reached asymptotically if $\dot{V}$ is negative definite. We have

$$\begin{aligned}\dot{V} &= \sigma_1\dot{\sigma}_1 \\ &= \sigma_1(\dot{x}_2 + (\bar{\lambda}_1|x_1 - z|^{\gamma_1 - 1} + \bar{\lambda}_2|x_1 - z|^{\gamma_2 - 1})(x_2 - \dot{z})) \\ &= \sigma_1(f_1(\mathbf{x}, t) + b_1(\mathbf{x}, t)u(t) + d_1(t) + (\bar{\lambda}_1|x_1 - z|^{\gamma_1 - 1} + \bar{\lambda}_2|x_1 - z|^{\gamma_2 - 1})(x_2 - \dot{z})).\end{aligned} \tag{24}$$

It can be easily shown from (24) that if u has the following form, $\dot{V}$ can be negative definite:

$$u = \hat{u} - Ksat(\sigma_1 b_1(\mathbf{x}, t)/\Phi_1), K > d/|b_1(\mathbf{x}, t)|, \tag{25}$$

where

$$\begin{aligned}\hat{u} = &-\frac{1}{b_1(\mathbf{x}, t)}\Big[f_1(\mathbf{x}, t) + (\bar{\lambda}_1|x_1 - z|^{\gamma_1 - 1} + \bar{\lambda}_2|x_1 - z|^{\gamma_2 - 1})(x_2 - \dot{z}) \\ &+ k_1\sigma_1 + k_2|\sigma_1|^\rho sign(\sigma_1)\Big], \\ sat(x) = &\begin{cases} sign(x), & \text{if } |x| \geq 1 \\ x, & \text{if } |x| < 1 \end{cases}, \quad z = sat(\sigma_2/\Phi_z),\end{aligned} \tag{26}$$

and Φ_z is a positive design parameter.

When $\sigma_1 = 0$ and $x_2 = -\lambda_1 sig^{\gamma_1}(x_1 - z_0) - \lambda_2 sig^{\gamma_2}(x_1 - z_0)$, x_1 will reach the setting point z_0 in finite time, where $z_0 = z(t_r)$ and t_r is the moment when $\sigma_1 = 0$. From the definition of saturation function (26), we can infer that $z = \sigma_2 = x_4 + \lambda_3 sig^{\gamma_3}(x_3) + \lambda_4 x_3 = 0$ when $z \leq \Phi_z$. The sliding surface σ_2 will reach zero in finite time which can also be seen in Figure 1; thus states x_3 and x_4 will go to zero.

From the discussion mentioned above, we can deduce the following theorem:

Theorem 3.1. *For the under-actuated system (1)-(4), the subsystem A is given by (5)-(6), and the subsystem B is given by (7)-(8). The fast decoupled terminal sliding surface functions are defined by (22). By introducing an intermediate variable z, both σ_1 and σ_2 converge to 0 if the control input u is given by (25).*

The fast decoupled terminal sliding surface functions with s_1 and s_3 (FDSMC13) are described in the following form:

$$\begin{aligned}\sigma_1 =& x_2 + \lambda_1 sig^{\gamma_1}(x_1 - z) + \lambda_2 sig^{\gamma_2}(x_1 - z), \\ \sigma_2 =& x_4 + \lambda_3 sig^{\gamma_3}(x_3),\end{aligned} \tag{27}$$

where $\gamma_1 > 1$, $1 < \gamma_2 < 2$ and $1 < \gamma_3 \leq 2$. Similar to the case of fast decoupled terminal sliding surface functions with s_1 and s_2, the control input of the FDTSMC13 is given by

$$\begin{aligned}u &= \hat{u} - Ksat(\sigma_1 b_1(\mathbf{x}, t)/\Phi_1), \\ \hat{u} &= \frac{1}{b_1(\mathbf{x}, t)}\Big[-(\bar{\lambda}_1|x_1 - z|^{\gamma_1 - 1} + \bar{\lambda}_2|x_1 - z|^{\gamma_2 - 1})(x_2 - \dot{z}) \\ &\quad - k_1\sigma_1 - k_2|\sigma_1|^\rho sign(\sigma_1) - f_1(\mathbf{x}, t)\Big], \ z = sat(\sigma_2/\Phi_z).\end{aligned} \tag{28}$$

Similarly, we also have the following theorem:

Theorem 3.2. *For the under-actuated system (1)-(4), the subsystem A is given by (5)-(6), and the subsystem B is given by (7)-(8). The fast decoupled terminal sliding surface functions are defined by (27). Sliding surfaces σ_1 and σ_2 will converge to zero if the control input u is given by (28).*

Proof: The proof of Theorem 3.2 is similar to the Theorem 3.1, and we omitted here.

4. **Simulation Study.** In order to verify the theoretical considerations and show the effectiveness of the proposed control schemes, a cart-pole system and TORA system are adopted and comparisons between the proposed method and the existing decoupled methods are presented.

4.1. **Cart-pole system.** The dynamic behavior of cart-pole system is given by (1)-(4), and

$$f_1(\mathbf{x},t) = \frac{m_t g \sin x_1 - m_p x_2^2 L \sin x_1 \cos x_1}{L(4m_t/3 - m_p \cos^2 x_1)}, \tag{29}$$

$$b_1(\mathbf{x},t) = \frac{3\cos x_1}{L(4m_t - 3m_p \cos^2 x_1)}, \tag{30}$$

$$f_2(\mathbf{x},t) = \frac{-4/3 m_p L x_2^2 \sin x_1 + m_p g \sin(2x_1)/2}{L(4m_t/3 - m_p \cos^2 x_1)}, \tag{31}$$

$$b_2(\mathbf{x},t) = \frac{4}{4m_t - 3m_p \cos^2 x_1}, \tag{32}$$

where $x_1(t)$ is the angular position of the pole from the vertical axis, $x_2(t)$ is the angular velocity of the pole with respect to the vertical axis, $x_3(t)$ is the position of the cart, $x_4(t)$ is the velocity of the cart, and L is the half-length of the pole. Mass of the system is $m_t = m_c + m_p$, where m_p is the mass of the pole, and m_c the mass of the cart. The state variables x_1 and x_2 are used to form the subsystem A (secondary target) and the state variables x_3 and x_4 are used to form the subsystem B (primary target). In the simulation study, the system state is assumed to be $\mathbf{x}_0 = [-\pi/6, 0, 0, 0]^T$ and the following parameters are used for the cart-pole system

$$m_p = 0.05\,\text{kg},\ m_c = 1\,\text{kg},\ L = 0.5\,\text{m},\ |d_1| = |d_2| \le 0.0873,\ g = 9.81\,\text{m/s}^2.$$

The sliding surfaces for FDTSMC12 and FDTSMC13 are defined by (22) and (27), and control laws are given by (25) and (28), respectively. In the simulation, the following fine-tune specifications are used:

$$\begin{aligned}
\text{NDTSMC: } & G_3 = G_4 = 0.05, G_5 = 5, G_8 = 0.5, K_1 = 6, k_1 = 2,\\
& k_2 = 5, \gamma_1 = \gamma_2 = 19/21.\\
\text{FDTSMC12: } & \lambda_1 = 5, \lambda_2 = 1, \lambda_3 = \lambda_4 = 0.5, K_1 = 5, k_1 = 2, k_2 = 5,\\
& \Phi_1 = 5, \Phi_z = 10, \gamma_1 = \gamma_3 = 21/19, \gamma_2 = 7/5, \rho = 5/7.\\
\text{FDTSMC13: } & \lambda_1 = \lambda_2 = 5, \lambda_3 = 0.8, K_1 = 5, k_1 = 10, k_2 = 8, \Phi_1 = 5,\\
& \Phi_z = 10, \gamma_1 = \gamma_3 = 21/19, \gamma_2 = 7/5, \rho = 5/7.
\end{aligned}$$

Comparing the control law of the NDTSMC, FDTSMC12 and FDTSMC13 for the cart-pole system, the states of the cart-pole system are depicted in Figures 2(a)-2(d). Both the convergence speed of FDTSMC12 and FDTSMC13 are faster than NDTSMC. As we observed in Figure 3(b), the effort of FDTSMC12 is a little bigger than NDTSMC, and FDTSMC13 has some overshot. We can see the newly proposed methods obtain better results even the fuzzy rule based approach is not employed. Here, we also need to emphasize that all the simulation limits the control effort in the range -40 N to 40 N,

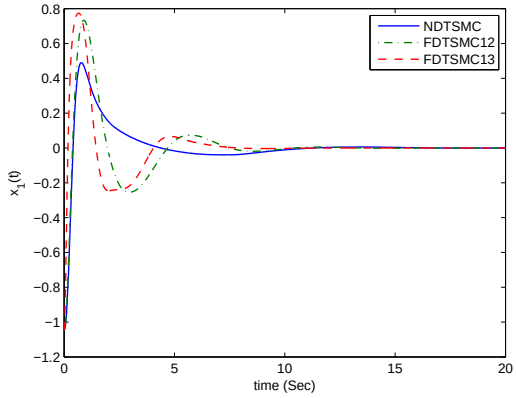

(a) Position of the pole

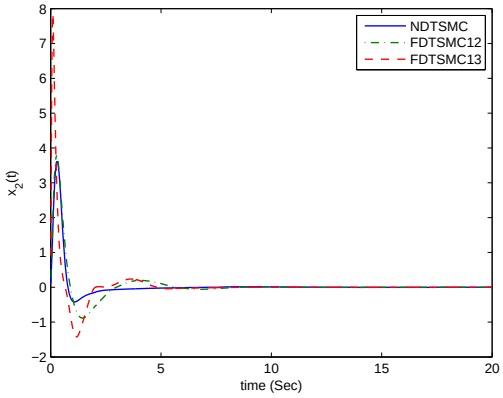

(b) Angular velocity of the pole

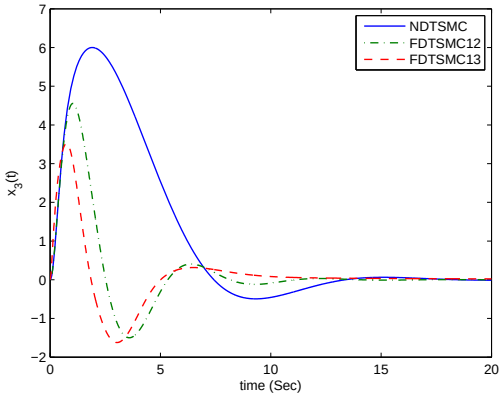

(c) Position of the cart

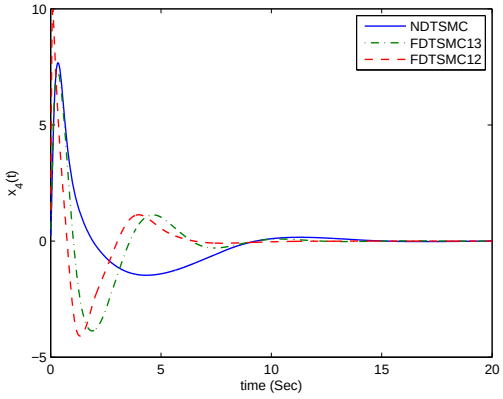

(d) Velocity of the cart

FIGURE 2. States for the cart-pole system using the NDTSMC, FDTSMC12 and FDTSMC13

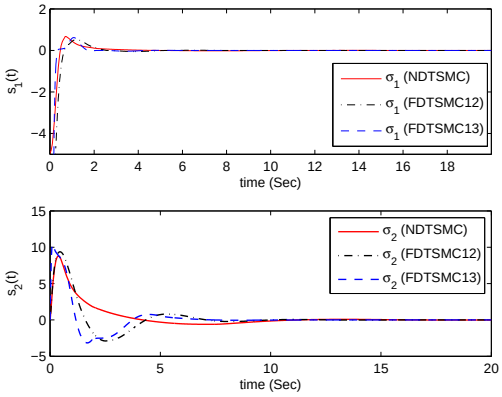

(a) Sliding surfaces for the subsystems A and B

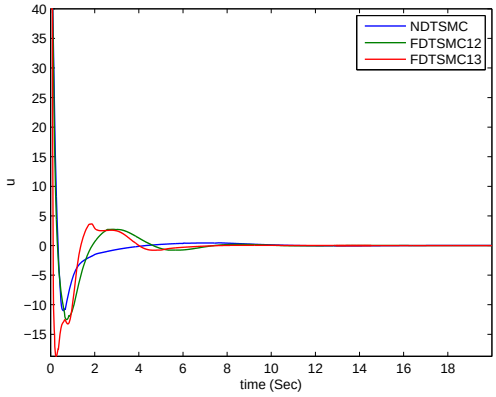

(b) Control input

FIGURE 3. Control effort and sliding surfaces for the cart-pole system using the NDTSMC, FDTSMC12 and FDTSMC13

since this is more applicable to the real practice. The sliding surfaces are shown in Figure 3(a).

4.2. **TORA system.** TORA system was introduced by Wan et al. [18], and has been extensively used as a test bed for nonlinear controllers, mainly for passivity based approaches [10]. The dynamics of the TORA can be described as follows:

$$\begin{aligned}
\dot{x}_1 &= x_2, \\
\dot{x}_2 &= -x_1 + \epsilon \sin x_3 + F_d, \\
\dot{x}_3 &= x_4, \\
\dot{x}_4 &= -\frac{\epsilon \cos x_3}{1 - \epsilon^2 \cos^2 x_3}(x_1 - \epsilon(1 + x_4^2)\sin x_3 - F_d) + \frac{u}{1 - \epsilon^2 \cos^2 x_3},
\end{aligned} \tag{33}$$

where $\epsilon = 0.1$, x_3 is the rotation angle which is defined as our main target, F_d represents disturbance force acting on the cart and u is control input. The sliding surfaces for the FDTSMC12 and FDTSMC13 are given as below respectively

$$\begin{cases} \sigma_1 = x_2 + \lambda_1 sig^{\gamma_1}(x_1) + \lambda_2 x_1, \\ \sigma_2 = x_4 + \lambda_3 sig^{\gamma_3}(x_3 - z) + \lambda_4 sig^{\gamma_4}(x_3 - z). \end{cases} \tag{34}$$

$$\begin{cases} \sigma_1 = x_2 + \lambda_1 sig^{\gamma_1}(x_1), \\ \sigma_2 = x_4 + \lambda_3 sig^{\gamma_3}(x_3 - z) + \lambda_4 sig^{\gamma_4}(x_3 - z). \end{cases} \tag{35}$$

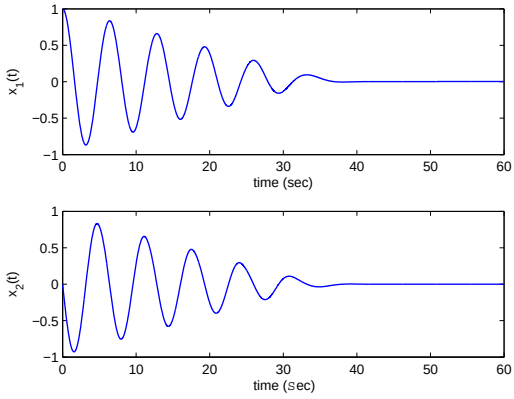

(a) Response of states x_1 and x_2

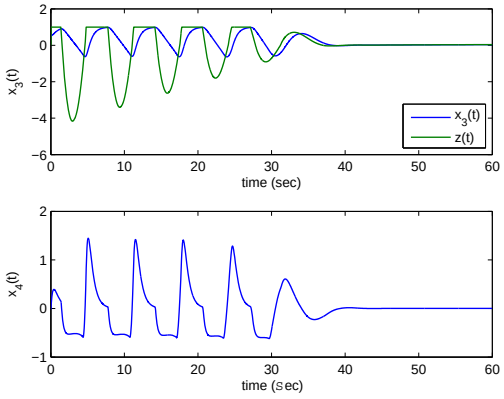

(b) Response of states x_3, x_4 and the intermediate variable z

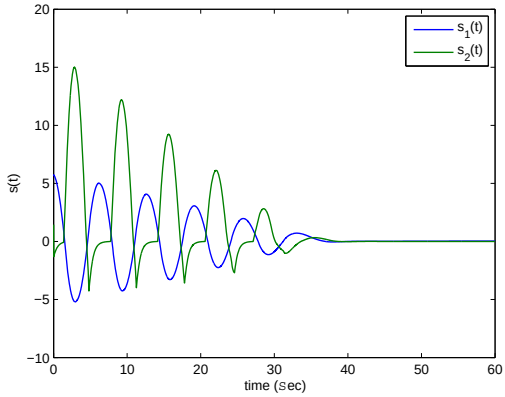

(c) Sliding surfaces of the subsystems A and B

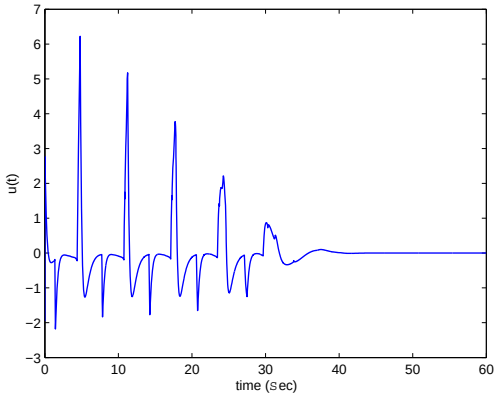

(d) Control input

FIGURE 4. The NDTSMC control results for the TORA system

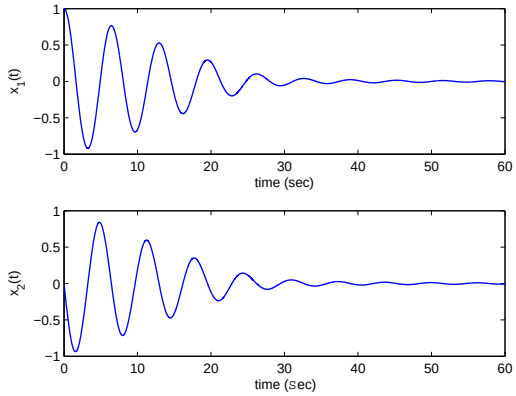

(a) Response of states x_1 and x_2

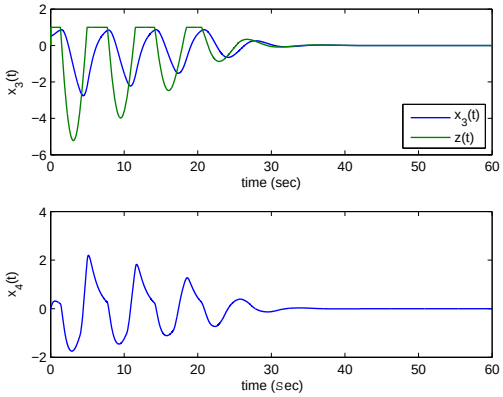

(b) Response of states x_3, x_4 and the intermediate variable z

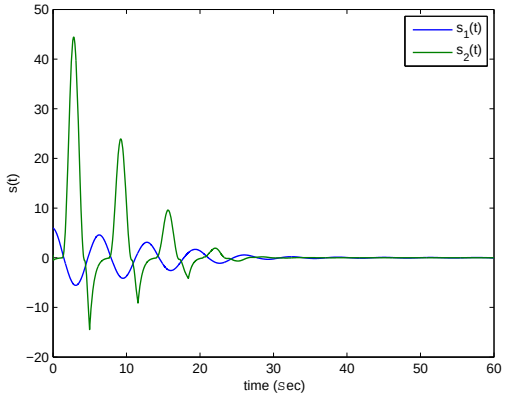

(c) Sliding surfaces of the subsystems A and B

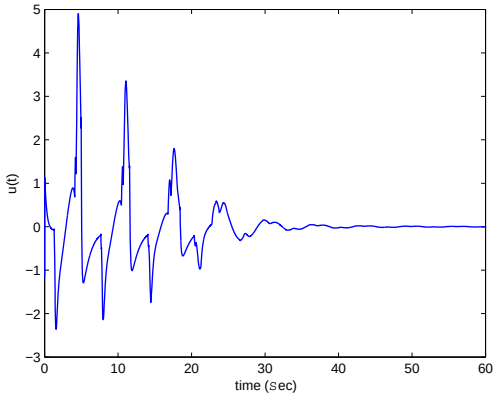

(d) Control input

FIGURE 5. The FDTSMC12 control results for the TORA system

The control input of FDTSMC12 and FDTSMC13 can be written as

$$\begin{aligned} u = &-\frac{(\bar{\lambda}_3|x_3 - z|^{\gamma_3 - 1} + \bar{\lambda}_4|x_3 - z|^{\gamma_4 - 1})x_4 - f_2(\mathbf{x}, t)}{b_2(\mathbf{x}, t)} \\ &- \frac{k_1\sigma_2 + k_2 sig^{\rho}(\sigma_2)}{b_2(\mathbf{x}, t)} - K sat(\sigma_2 b_2(\mathbf{x}, t), \Phi_1), \ \ z = sat(\sigma_1/\Phi_z), \end{aligned} \tag{36}$$

where

$$f_2(\mathbf{x}, t) = -\epsilon \cos x_1 (x_1 - \epsilon(1 + x_2)^2) \sin x_1 / (1 - \epsilon^2 \cos^2 x_1), \tag{37}$$

$$b_2(\mathbf{x}, t) = 1/(1 - \epsilon^2 \cos^2 x_1). \tag{38}$$

Let the initial value of x be $[1, 0, \pi/6, 0]^T$; the following fine-tune simulation parameters are specified:

$$\begin{aligned} \text{NDTSMC: } & G_3 = G_4 = 0.05, G_5 = 6, G_6 = G_7 = 0.05, G_8 = 3, \\ & K_1 = 2, \Phi_1 = \Phi_z = 1, \gamma_1 = \gamma_2 = 19/21. \\ \text{FDTSMC12: } & \lambda_1 = \lambda_3 = 3, \lambda_4 = 1, K = 0.8, k_1 = k_2 = 0.5, \Phi_1 = 1, \\ & \Phi_z = 1, \gamma_1 = \gamma_3 = 21/19, \gamma_4 = 5/3, \rho = 3/7. \\ \text{FDTSMC13: } & \lambda_1 = 6, \lambda_3 = \lambda_4 = 1, K = 1, k_1 = k_2 = 0.5, \Phi_1 = \Phi_z = 1, \\ & \gamma_1 = \gamma_3 = 21/19, \gamma_4 = 7/5, \rho = 5/7. \end{aligned}$$

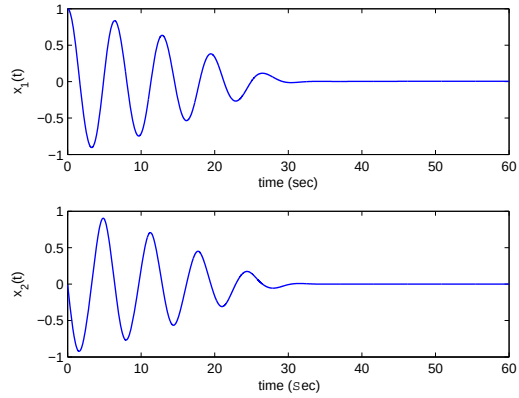

(a) Response of states x_1 and x_2

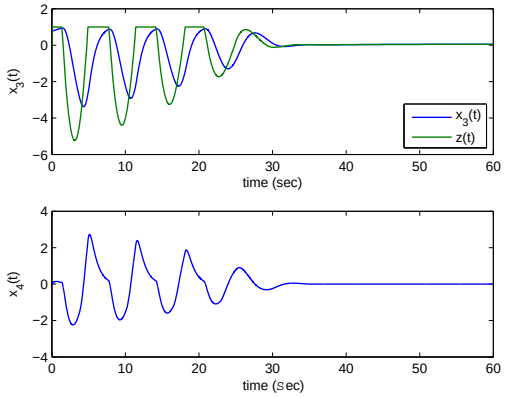

(b) States x_3, x_4 and intermediate variable z

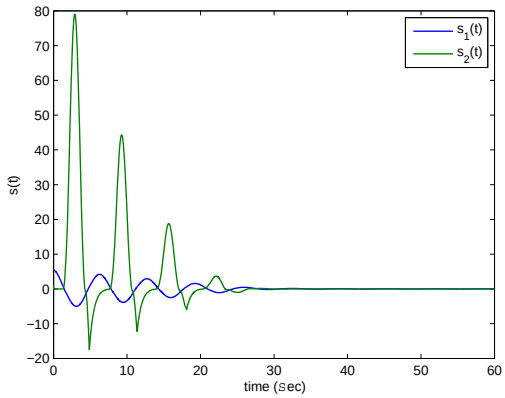

(c) Sliding surfaces of the subsystems A and B

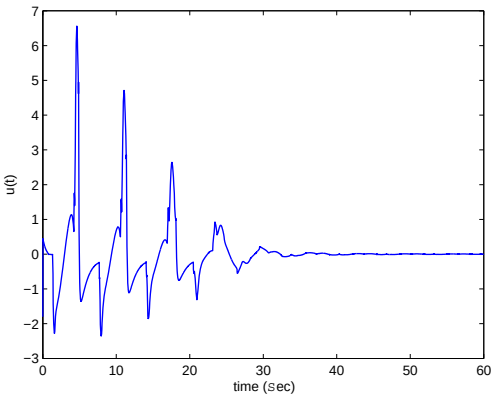

(d) Control input

FIGURE 6. The FDTSMC13 control results for the TORA system

Figures 4(a)-4(d) show the simulation results of the NDTSMC, Figure 4(a) shows that the state x_1 can reach the zero at about 37 s, x_3 can reach the zero at about 38 s, which is shown in Figure 4(b). From Figures 5(a)-5(b) and Figures 6(a)-6(b), the states exhibit faster response than NDTSMC. Figures 4(c), 5(c) and 6(c) show the sliding surfaces of the TORA system. It is evident that the plots obtained by the FDTSMC12 and FDTSMC13 confirm the behavior of the sliding surface functions converging to zero in finite time. The control input in 5(d) and 6(d) obtained by FDTSMC12 and FDTSMC13 are smaller than that of NDTSMC which is shown in Figure 4(d).

4.3. **Experimental results of cart-pole system.** In this section, we present experimental results obtained on a portable cart-pole system. The experimental apparatus is shown in Figure 7 (left). The model parameters used are shown in Table 1.

TABLE 1. Parameters for the cart-pole system

Parameter	Value	Units
L	0.175	m
m_c	0.411	kg
m_p	0.078	kg

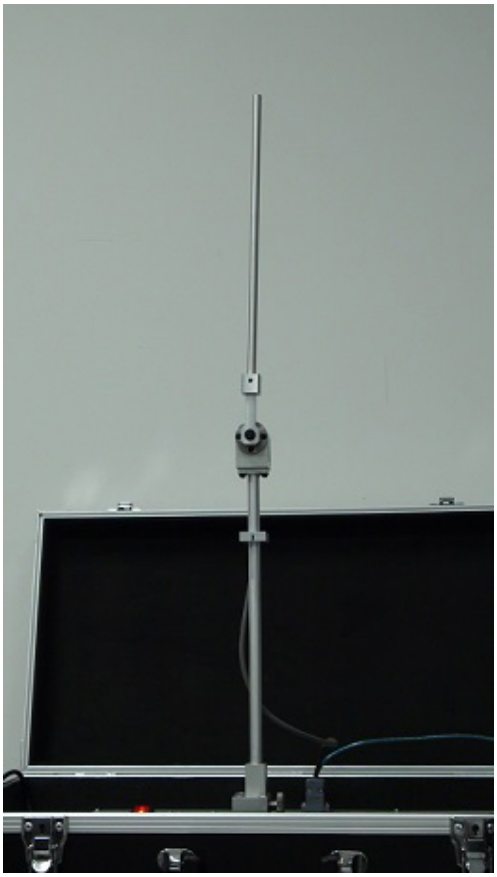

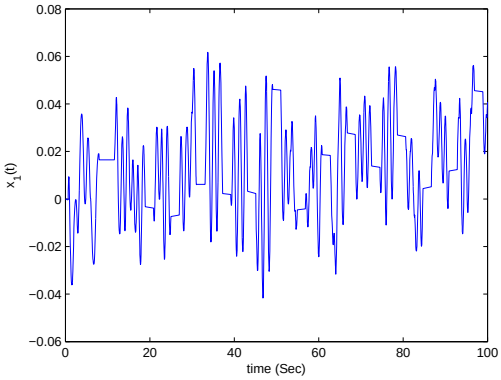

(a) Position of cart-pole system

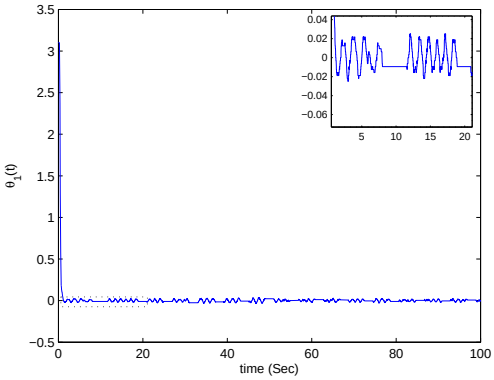

(b) Angular position of cart-pole system

FIGURE 7. Portable cart-pole system (left) and experimental results of FDTSMC12 for the cart-pole system (right)

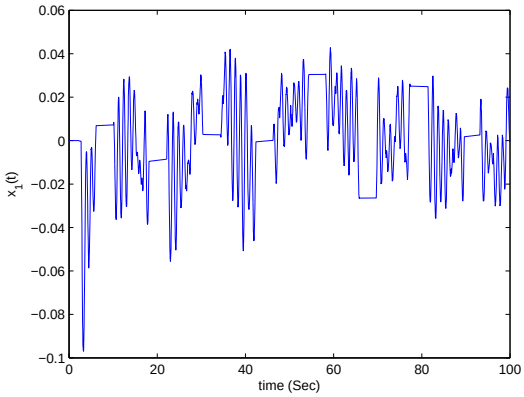

(a) Position of cart-pole system

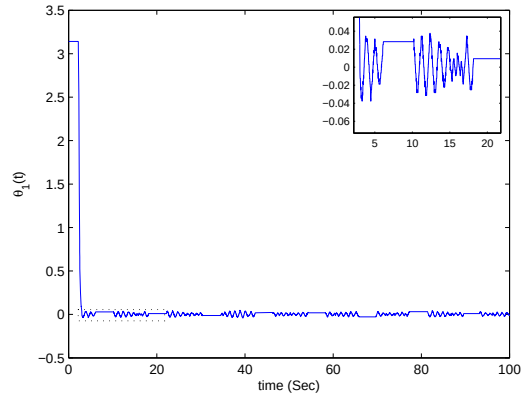

(b) Angular position of cart-pole system

FIGURE 8. The experimental results of FDTSMC13 for the cart-pole system

The apparatus has a 500 count/rev encoder fitted to each axis. The controller was implemented in Simulink with the RTBlock which can be downloaded from matlab central. Angular rates were estimated by a first-order difference with no filtering. We verify the newly proposed controller with initial state $\mathbf{x}_0 = [0, 0, \pi, 0]^T$ and the disturbances and friction are omitted. The pole is manually raised to the vertical position, and the fast

decoupled terminal sliding mode controller is activated. Position of cart-pole system using FDTSMC12 is shown in Figure 7(a). Angular velocity of cart-pole system is shown in Figure 7(b). Position and angular velocity of cart-pole system using FDTSMC13 are shown in Figure 8(a) and Figure 8(b), respectively.

We can see in the figures that both the FDTSMC12 and FDTSMC13 can stabilize the cart-pole system successfully. Moving range of FDTSMC12 is relatively larger than FDTSMC13, which is due to the fact that FDTSMC12 (with sliding surfaces s_1 and s_2) has a faster convergence speed than FDTSMC13 (with sliding surfaces s_1 and s_3). There exists a little chattering around the vertical position with both the FDTSMC12 and FDTSMC13 which are shown in Figure 8(a) and Figure 8(b). However, the chattering is small.

5. **Conclusions and Future Work.** Two fast decoupled terminal sliding mode control methods using hybrid sliding surfaces are proposed for a class of under-actuated nonlinear systems. Hybrid sliding surfaces are utilized to get a faster convergence speed. Compared with the existing decoupled terminal sliding control methods, this approach offers a simplified structure, easy implementation and high precision control scheme. The approach eliminates the need for using fuzzy rules, and has no degradation in performance at the same time. Simulation and experimental results of a cart-pole system with the proposed control methods demonstrate that the dynamic response is faster than other nonsingular decoupled terminal sliding control methods. In addition, the effectiveness of the proposed methods is also verified by TORA system. However, since the proposed method is based on using a two-level decoupling control strategy, it is difficult for the existing decoupled methods to extend to the higher-order under-actuated systems where the order is higher than four. The newly proposed approach has the potential application in the higher-order terminal sliding mode control problem, since the sliding surfaces can be modified to the higher-order case, the modified sliding surface will be $s_1 = \dot{x} + \lambda_1 sig^{\gamma_1}(x_1 - z_1) + \lambda_2 sig^{\gamma_2}(x_1 - z_2)$, where z_1 and z_2 are the intermediate variables for the other two subsystems. Our future work is to study the stabilization and swing up problems of higher-order under-actuated system such as double-inverted pendulum and its experiment implementation.

Acknowledgement. The authors would like to thank the editors and anonymous reviewers for their insightful comments. The authors are also grateful for the support by the National Natural Science Foundation of China under Grant (61104038, 61374118), China Postdoctoral Science Foundation funded project (2013M541233) and the Major Industrialization Programs of Harbin (2012BD2BG041).

REFERENCES

[1] H. M. Zhang, X. W. Ma, W. Xu and P. Z. Wang, Design fuzzy controllers for complex systems with an application to 3-stage inverted pendulums, *Information Sciences*, vol.72, no.3, pp.271-284, 1993.

[2] J. C. Lo and Y. Kuo, Decoupled fuzzy sliding-mode control, *IEEE Transactions on Fuzzy Systems*, vol.6, no.3, pp.426-435, 1998.

[3] L. C. Hung and H. Y. Chung, Decoupled sliding-mode with fuzzy-neural network controller for nonlinear systems, *International Journal of Approximate Reasoning*, vol.46, no.1, pp.74-97, 2007.

[4] A. Bagheri and J. J. Moghaddam, Decoupled adaptive neuro-fuzzy (DANF) sliding mode control system for a lorenz chaotic problem, *Expert Systems with Applications*, vol.36, no.3, pp.6062-6068, 2009.

[5] L. C. Hung, H. P. Lin and H. Y. Chung, Design of self-tuning fuzzy sliding mode control for TORA system, *Expert Systems with Applications*, vol.32, no.1, pp.201-212, 2007.

[6] L. Wu, X. Su and P. Shi, Sliding mode control with bounded L_2 gain performance of Markovian jump singular time-delay systems, *Automatica*, vol.48, no.8, pp.1929-1933, 2012.

[7] M. Liu, P. Shi, L. Zhang and X. Zhao, Fault tolerant control for nonlinear Markovian jump systems via proportional and derivative sliding mode observer, *IEEE Transactions on Circuits and Systems I*, vol.58, no.11, pp.2755-2764, 2011.

[8] L. Wu, P. Shi and H. Gao, State estimation and sliding mode control of Markovian jump singular systems, *IEEE Transactions on Automatic Control*, vol.55, no.5, pp.1213-1219, 2010.

[9] J. Zhang, P. Shi and Y. Xia, Robust adaptive sliding mode control for fuzzy systems with mismatched uncertainties, *IEEE Transactions on Fuzzy Systems*, vol.18, no.4, pp.700-711, 2010.

[10] M. Jankovic, D. Fontaine and P. V. Kokotovi, TORA example: Cascade and passivity based control designs, *IEEE Transactions on Control Systems Technology*, vol.4, no.3, pp.292-297, 1996.

[11] F. Y. Cheng, G. M. Zhong, Y. S. Li and Z. M. Xu, Fuzzy control of a double-inverted pendulum, *Fuzzy Sets and Systems*, vol.79, no.3, pp.315-321, 1996.

[12] Y. Becerikli and B. K. Celik, Fuzzy control of inverted pendulum and concept of stability using java application, *Mathematical and Computer Modelling*, vol.46, no.1-2, pp.24-37, 2007.

[13] T. Holzhüter, Optimal regulator for the inverted pendulum via Euler-Lagrange backward integration, *Automatica*, vol.40, no.9, pp.1613-1620, 2004.

[14] K. Graichen, M. Treuer and M. Zeitz, Swing-up of the double pendulum on a cart by feedforward and feedback control with experimental validation, *Automatica*, vol.43, no.1, pp.63-71, 2007.

[15] H. Bayramoglu and H. Komurcugil, Nonsingular decoupled terminal sliding-mode control for a class of fourth-order nonlinear systems, *Communications in Nonlinear Science and Numerical Simulation*, vol.18, no.9, pp.2527-2539, 2013.

[16] S. H. Li, Z. Wang and S. M. Fei, Finite-time control of a bioreactor system using terminal sliding mode, *International Journal of Innovative Computing, Information and Control*, vol.5, no.10, pp.3495-3504, 2009.

[17] S. Chen, F. Yu and H. Chung, Decoupled fuzzy controller design with single-input fuzzy logic, *Fuzzy Sets and Systems*, vol.129, no.3, pp.335-342, 2002.

[18] C. J. Wan, D. S. Bernstein and V. T. Coppola, Global stabilization of the oscillating eccentric rotor, *Nonlinear Dynamics*, vol.10, no.1, pp.49-62, 1996.

[19] L. Yang and J. Yang, Nonsingular fast terminal sliding-mode control for nonlinear dynamical systems, *International Journal of Robust and Nonlinear Control*, vol.21, no.16, pp.1865-1879, 2011.

[20] M. Abramowitz and I. Stegun, Handbook of mathematical functions with formulas, graphs, and mathematical tables, *National Bureau of Standards Applied Mathematics*, vol.55, Dover, New York, USA, 1972.

[21] G. Oriolo and Y. Nakamura, Control of mechanical systems with second-order nonholonomic constraints: Underactuated manipulators, *Proc. of the 30th IEEE Conference on Decision and Control*, Brighton, UK, pp.2398-2403, 1991.

[22] M. Jankovic, D. Fontanie and P. V. Kokotovic, TORA example: Cascade and passivity based control designs, *IEEE Transacitons on Control System Technology*, vol.4, no.3, pp.292-297, 1996.

[23] R. Olfati-Saber, Normal forms for underactuated mechanical systems with symmetry, *IEEE Transactions on Automatic Control*, vol.47, no.2, pp.305-308, 2002.

[24] E. Altug, J. P. Ostrowski and R. Mahony, Control of a quadrotor helicopter using visual feedback, *Proc. of the 2002 IEEE International Conference on Robotics and Automation*, Washington, USA, pp.72-77, 2002.

[25] J. Hauser, S. Satry and P. Kokotovic, Nonlinear control via apprximate input-output linearization: The ball and beam example, *IEEE Transactions on Automatic Control*, vol.37, no.3, pp.392-398, 1992.